Pharm Res (2014) 31:2904–2917
DOI 10.1007/s11095-014-1386-3

RESEARCH PAPER

Incorporation of Ophiobolin A into Novel Chemoembolization Particles for Cancer Cell Treatment

Rachel Morrison • Chris Gardiner • Antonio Evidente • Robert Kiss • Helen Townley

Received: 15 January 2014 / Accepted: 7 April 2014 / Published online: 3 May 2014

ABSTRACT

Purpose To design and synthesize chemoembolization particles for the delivery of Ophiobolin A (OphA), a promising fungal-derived chemotherapeutic, directly at the tumour location. To investigate cell death mechanism of OphA on a Rhabdomyosarcoma cancer (RD) cell line. Rhabdomyosarcoma is the most common soft tissue sarcoma in children; with a 5-year survival rate of between 30 and 65%.

Methods Multimodal chemoembolization particles were prepared by sintering mesoporous silica nanoparticles, prepared by the sol-gel method, onto the surface of polystyrene microspheres, prepared by suspension copolymerisation. The chemoembolization particles were subsequently loaded with OphA. The effects of OphA *in vitro* were characterised by flow cytometry and nanoparticle tracking analysis (NanoSight).

Results High loading of OphA onto the chemoembolization particles was achieved. The subsequent release of OphA onto RD cells in culture showed a 70% reduction in cell viability. OphA caused RD cells to round up and their membrane to bleb and caused cell death via apoptosis. OphA caused both an increase in the number of microvesicles produced and an increase in DNA content within these microvesicles.

Conclusions The prepared chemoembolization particles showed good efficacy against RD cells in culture.

KEY WORDS cancer · chemoembolization · mesoporous silica · microvesicles · Ophiobolin A

ABBREVIATIONS

AIBN	Azobisisobutyronitrile
CTAB	Cetyl trimethylammonium bromide
CytoD	CytochalasinD
DCM	Dichloromethane
DMEM	Dulbecco's Modified Eagle's Medium
EGDMA	Ethylene glycol dimethacrylate
Em	Emission
Ex	Excitation
GFP	Green fluorescent protein
HMSNP	Hexagonal mesoporous silica nanoparticles
LC	Liquid chromatography
mtDNA	Mitochondrial DNA
NTA	Nanoparticle tracking analysis
OphA	Ophiobolin A
PBS	Phosphate buffered saline
PI	Propidium iodide
PS	Polystyrene spheres
PS-HMSNP	Polystyrene-(hexagonal mesoporous silica nanoparticle) composite particles
PVA	Poly(vinyl alcohol)
RD	Rhabdomyosarcoma cancer cell line
RMS	Rhabdomyosarcoma
SD	Standard deviation
SEM	Scanning electron microscopy
TEM	Transmission electron microscopy
TEOS	Tetraethyl orthosilicate

Electronic supplementary material The online version of this article (doi:10.1007/s11095-014-1386-3) contains supplementary material, which is available to authorized users.

R. Morrison · H. Townley (✉)
Department of Engineering Science, Oxford University, Parks Road Oxford, UK
e-mail: helen.townley@eng.ox.ac.uk

C. Gardiner · H. Townley
Nuffield Department of Obstetrics and Gynaecology, John Radcliffe Hospital, Oxford University, Oxford, UK

A. Evidente
Dipartimento di Scienze Chimiche, Università di Napoli Federico II Complesso Universitario Monte Sant'Angelo, Via Cintia 4
80126 Napoli, Italy

R. Kiss
Laboratoire de Cancérologie et de Toxicologie Expérimentale, Faculté de Pharmacie, Université Libre de Bruxelles, Brussels, Belgium

INTRODUCTION

Combining chemotherapy drugs with embolic particles has been shown to have a synergistic effect on the reduction of tumour size (1). Herein we describe the design and synthesis of a new embolic particle, and combination with a novel chemotherapeutic. Embolic particles can be introduced in to the blood stream close to the target, and by lodging in the small vessels which feed the tumour restrict the nutrient and oxygen supply shrink the tumour (2). Incorporation of chemotherapeutic drugs into an embolization particle (chemoembolization) also allows a drug to be delivered directly to the cancerous cells, and whereas systemic chemotherapy delivers the drug into the bloodstream and exposes the whole body to the toxic effects of the compound, chemoembolization hones in on the site of the cancerous cells. The embolic particles in this study were designed to have a high surface area for maximal drug loading. Spherical microparticles were therefore coated with mesoporous silica nanoparticles which have a nanoporous structure for a high loading capacity. Silica is known to have good biocompatibility, and could be further functionalized if desired with, for example, peptides or siRNA (3). The pores are also tunable to the size of the particular drug to be delivered for maximum loading and unloading (4).

The agent chosen for investigation and incorporation into the chemoembolic particles was a fungal phytotoxic derived compound, Ophiobolin A (OphA). OphA is a secondary metabolite produced by the pathogenic fungi *Bipolaris* species which is known to attack rice, maize and sorghum to produce brown spot lesions (5). This sestertepene-type compound (C25) is one of a group of over 25 ophiobolin analogues which all feature a unique tricyclic chemical structure (Fig. 1). Historically, much of the research on ophiobolins focused on their effects on plants showing that they cause rapid disorganisation of the plant cell membrane resulting in electrolyte and sugar leakage, (6) and inhibition of calmodulin-activated cyclic nucleotide phosphodiesterase (7). More recently, OphA has been shown to exhibit a broad spectrum of inhibitory activity *in vitro* on various cancer cell lines including A549 (lung cancer), SKMEL28 (melanoma), Hs683 (brain cancer), and OVCAR3 (ovarian cancer) (8,9). IC_{50} values were found to vary between 0.28 and 0.62 μM after 3 days treatment. We therefore wanted to investigate whether OphA might be effective in treating rhabdomyosarcoma (RMS); a cancer of the connective tissue most commonly found in young children and adolescents. RMS may occur in many places in the body, although the most common sites are structures of the head and neck, the urogenital tract, and the arms or legs. There is precedent for the use of preoperative arterial embolization in cases of RMS, for example, in uterine RMS, (10) perineal RMS (11) and resection of an orbital RMS (12).

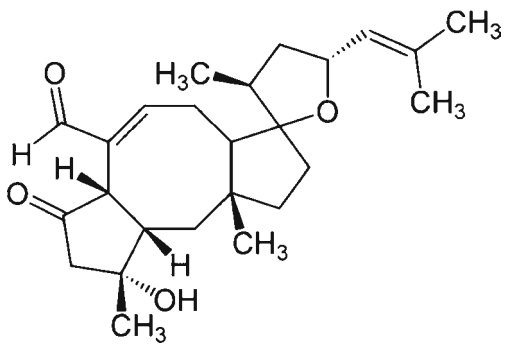

Fig. 1 Chemical structure of Ophiobolin A.

While the mechanism of OphA on plants has been studied extensively, the interaction with mammalian cells is not well understood. It has been observed in U373-MG (brain cancer) cells that vacuolization occurs and that these vacuoles are ejected from the surface of the cells over time (13). The expulsion of microvesicles from RMS cells after treatment with OphA was therefore quantified and characterized. Such extracellular microvesicles are released by most cells and encompass three main types: (i) exosomes (40–100 nm) which are constitutively released by the exocytosis of multivesicular bodies (ii) shedding microvesicles (50–1000 nm) which arise due to the direct budding of the plasma membrane and (iii) apoptotic bodies (50–5000 nm) which are produced during apoptosis and contain cellular content and organelles (14).

This study therefore investigates the cell death mechanisms induced in an RMS cell line, and the concomitant release of microvesicles. Furthermore, the development of an embolic particle is described to give high drug carrying capacity for slow release of a drug in close proximity to the tumour, and the efficacy of delivering OphA in such a chemoembolic particle is investigated.

MATERIALS AND METHODS

Synthesis of Drug Delivery System

Mesoporous Silica with Hexagonal-Symmetry (HMSNP)

Synthesis of mesoporous silica nanoparticles with hexagonal symmetry of the pores (HMSNP) was performed by a surfactant-templated base catalysed sol-gel reaction, as previously described by Hom *et al.* (15). Briefly, 100 mg of Cetyl trimethylammonium bromide (CTAB, Aldrich; 99%) was dissolved in 48 ml of ddH_2O and 350 μl of 2 M NaOH (Aldrich) and stirred at 500 rpm in a round bottomed flask. The mixture was heated to 80°C and once the temperature was stable, 0.5 ml of tetraethyl orthosilicate (TEOS; Aldrich) was added. After 15 min incubation, 127 μl of 3-(trihydroxysilyl) propyl

methylphosphonate was added. After a further 2 h incubation the nanoparticles were collected by centrifugation and washed twice in methanol (Rathburn). The nanoparticles were resuspended in 20 ml of methanol and 1 ml of 37% hydrochloric acid (Aldrich) and then refluxed overnight at 80°C to remove the CTAB. The nanoparticles were collected by centrifugation and washed in ethanol (Fisher) twice before drying under vacuum.

Polystyrene Spheres (PS)

Synthesis of polystyrene spheres (PS), for the core of the embolic particle, was performed by suspension copolymerisation of styrene and ethylene glycol dimethacrylate (EGDMA), as previously described by Ihara *et al.* (16,17). Briefly, 2.5 ml of styrene (Aldrich), 2.5 ml of EGDMA (Aldrich) and 50 mg of azobisisobutyronitrile (AIBN; Aldrich) were mixed to create an oil phase. The oil phase was added to the 30 ml of an aqueous phase containing 4 wt.% poly (vinyl alcohol) (PVA) (87–90% hydrolyzed, average molecular weight 30,000–70,000; Aldrich) in a round bottomed flask. The mixture was stirred at 250 rpm for one hour at room temperature and then left to stand for 24 h at 60°C. The particles were collected by centrifugation, washed in ddH_2O twice, resuspended in 30 ml ddH_2O and refluxed overnight to remove any remaining PVA. The particles were then collected by centrifugation, washed with methanol twice and dried under vacuum.

Coating of the Embolic Particle with HMSNP

The coating of the PS with HMSNP to create PS-HMSNP embolic particles was performed by mixing PS with (1:9 v/v) HMSNP. The mesoporous silica was then sintered onto the surface of the polysytrene spheres by heating the mixture to 230°C at a ramping rate of seven degrees per minute and then holding at 230°C for two hours in a Carbolite RWF 1200 furnace. The PS-HMSNP were separated from the excess HMSNP using a sucrose density gradient containing 60% and 15% sucrose. The gradient was centrifuged at 9,000 rpm for one hour and then the band containing the PS-HMSNP was extracted, centrifuged and washed in ddH_2O three times to remove sucrose. Finally the prepared PS-HMSNP particles were dried overnight under vacuum.

Particle Characterisation

HMSNP and PS-HMSNP were characterised using transmission and scanning electron microscopy (TEM and SEM), disc centrifugation and electokinetic (ζ) potential. TEM was used to measure the size, surface morphology and nanopores of the HMSNP. TEM was performed using a JEOL JEM-2010 microscope equipped with a LaB_6 thermionic electron gun operating at a primary beam energy of 200 keV. TEM specimens were prepared by resuspending the nanoparticles in ethanol and drop casting onto holey carbon coated grids (Agar Scientific).

SEM was used to evaluate the size and surface morphology of the HMSNP and the size distribution and surface coverage of the PS-HMSNP. SEM was performed using a JEOL JSM-840 F microscope operated at a primary beam energy of 3 kV and images were collected in secondary electron imaging mode. SEM specimens were prepared by dusting onto a carbon taped SEM stub (Agar Scientific) and then coated with a 3 nm layer of platinum. The platinum layer adds a conductive layer which reduces charging during operation.

The hydrodynamic size distribution was measured using a Disc Centrifuge (DC 18000; CPS instruments). The machine was operated at 24,000 rpm and a sucrose density gradient was prepared inside the disc. Samples (100 μl) were injected into the centre of the disc and from the time taken to reach the detector, the density of the particles and the rotation speed the size distribution can be calculated. Samples were calibrated against particles of a known diameter (Polyvinyl chloride, 0.377 μm, CPS instruments). Samples were prepared by resuspending the particles in ddH_2O and sonicating using an ultrasonic probe (Sonic Vibra-Cell) for 5 min (104 W, (80% amplitude and 5 s on/5 s off). The electrokinetic (ζ) potential was measured by electrophoretic light using a Malvern Zetasizer Nano. Samples were resuspended in ddH_2O buffered to physiological pH.

Ophiobolin A

Ophiobolin A (OphA) was obtained as white crystals from *Drechslera gigantea* culture filtrates according the procedure previously reported (18). The purity of OphA was determined by RP-HPLC-UV to be >95%.

Cell Culture

The biological effects of OphA were tested *in vitro* on RD cells (American Type Tissue Culture Collection; ATCC no. CCL-136). These are an embroyonal rhabdomysarcoma (ERMS) cell line; rhabdomysarcoma is the most common soft-tissue sarcoma found in children and adolescents. RD cells expressing green fluorescent protein (GFP) were prepared using a lentiviral vector to transfect RD cells with GFP following the modified method presented by Kafri *et al.* (19) (a kind gift from Xinyue Huang, Oxford University, UK).

Cells were grown in growth medium (Dulbecco's Modified Eagle's Medium (DMEM); Aldrich) supplemented with 10% fetal calf serum (Aldrich), 2 mM L-Glutamine (Aldrich), 100 U/ml Penicillin (Aldrich) and 0.1 mg/ml Streptomycin (Aldrich) and incubated at 37°C in a 5% CO_2 atmosphere. Cells were passaged every 3 to 4 days.

Flow Cytometry

RD cells expressing green fluorescent protein (GFP) were plated at a density of 8×10^4 cells per well (24 well plate) in 0.5 ml of growth media and incubated for 24 h. Subsequently cells were either incubated with (i) free OphA in phosphate buffered saline (PBS; Aldrich) at a concentration ranging from 0 to 100 μM, (ii) HMSNP loaded with OphA (3.5 mg nanoparticles containing between 330 and 835 μmoles of OphA depending on the solvent used for loading) and resuspended in growth media, (iii) PBS only as a control. Cells were incubated for a further 24 h.

The supernatant, containing the non-adherent cells, was removed to a microcentrifuge tube, the adherent cells were washed and trypsinized (Trypsin-EDTA; Aldrich) and then combined with the first supernatant. The combined cells were then centrifuged and washed in PBS, before being resuspended in 50 μl of annexin V binding buffer (BioLegend). Two fluorescent dyes were used to determine cell viability: propidium iodide (PI; Aldrich) and APC-Annexin V (Biolegend). PI (2.5 μl) and APC-Annexin V (2.5 μl) was added to the cells in the annexin V binding buffer and incubated in the dark at room temperature for 15 min. Subsequently 200 μl of binding buffer was added to the cells and then the samples were analysed by flow cytometry.

The samples were analysed using an Accuri C6 Flow Cytometer (BD). Gating was used to select the area containing GFP expressing RD cells and this area was used for further analysis. Fluorescence intensity of both the PI and the APC channels was used to determine the cells which were live, undergoing early apoptosis or were dead due to either apoptosis of necrosis. Quantitative analysis was conducted by determining the percentage of stained cells compared to the total number of cells. Experiments were performed in triplicate and repeated on three separate occasions.

Nanoparticle Tracking Analysis

Nanoparticle tracking analysis (NTA), using a NanoSight NS500 (Nanosight, Amesbury, UK) was used to monitor the release of microvesicles from the RD cells after treatment.

NanoSight

NTA uses a finely focused laser beam which illuminates the particles within the sample. The particles resident within the beam can be visualised using a conventional optical microscope, fitted with a video camera, which can detect the light scattered from the particles within the field of view. Five separate videos of 30 s were recorded at camera level 12 and then the particle movement due to Brownian motion was analysed using NTA 2.3 software (NanoSight). The velocity of the particle movement is used to calculate the particle size by applying the two- dimensional Stokes-Einstein Eq. 1:

$$< x,y>^2 = \frac{K_B T t_s}{3\pi\eta d_h} \quad (1)$$

where $<x,y>^2$ is the mean squared displacement, K_B is Boltzmann's constant, T is the temperature of the solvent in Kelvin, t_s is the sampling time, η is the viscosity and d_h is the hydrodynamic diameter.

NanoSight Sample Preparation

RD cells were plated at a density of 75×10^4 cells per flask (T25 flask) in 3 ml of OPTIMEM (Gibco) and allowed to attach to the flask for 24 h. OPTIMEM was used as it is a low serum media and therefore the background level of microvesicles was low and because the phenol red within DMEM was known to cause interference with the NTA. Subsequently cells were treated with 200 μl of (i) PBS only as a control, (ii) 1 μM OphA, (iii) 10 μM OphA, (iv) 1 μM OphA +5 μM CytochalasinD (CytoD; Aldrich), (v) 10 μM+ 5 μM CytoD, (vi) 5 μM CytoD. The cells were incubated for a further 24 h.

The size and concentration of the microvesicles released from the cells into the supernatant was measured using a NanoSight NS500. The microvesicles were diluted in PBS to ensure the concentration of particles was within the optimum range of $2–10\times10^8$ particles per ml for NanoSight measurement and then each sample was measured in light scatter mode. Experiments were repeated on three separate occasions.

Fluorescent Labelling of Microvesicles

The microvesicles were labelled with SYBR® green (Ex. 554 nm, Em. 567 nm; Life technologies), as a marker for DNA, and CellMask™ orange (Ex. 554 nm, Em. 567 nm; Life technologies), as a marker for plasma membrane. Microvesicles from the supernatant (250 μl) were incubated with either 10 μl of SYBR® green (×1000 stock solution) or 0.5 μl of 5 μg/ml CellMask™ orange for 30 min at 37°C, protected from light. The microvesicles were pelleted by centrifugation at 30,000 rpm for one hour and washed in PBS to remove any residual dye. Finally the cells were resuspended in 0.5 ml of PBS, centrifuged at 10,000 rpm for 10 min to pellet any cell debris whilst keeping the microvesicles in suspension before analysis by NTA.

The NanoSight NS500 equipped with a 488 nm laser has been adapted to allow for the detection of microvesicles labelled with fluorescent dyes. A 500 nm long pass filter is used so that only fluorescent emitted light can be measured. The fluorescent microvesicles are tracked in real time, similarly to conventional NTA analysis, and the microvesicles size,

concentration and fluorescence intensity can be determined. Under conventional light scatter mode the total number of particles can be determined and subsequently compared to the number of dyed microvesicles. Experiments were repeated on three separate occasions.

Loading of OphA into the HMSNP and PS-HMSNP

HMSNP (10 mg) were incubated in 2 ml of 0.5 mg/ml OphA in either dichloromethane (DCM; Aldrich), ethanol (Fisher) or toluene (Aldrich). Samples were agitated using a magnetic stirrer at 500 rpm for 3 days at room temperature. The samples were centrifuged at 12,000 rpm for 5 min to pellet the nanoparticles and the supernatant was removed. Finally the loaded HMSNP@OphA were dried overnight at 18°C under vacuum. A similar procedure was used for loading the PS-HMSNP with OphA.

The concentration of OphA remaining in the supernatant after loading was measured by liquid chromatography (LC). An Agilent LC 1120 Compact LC equipped with an Agilent Eclipse Plus C18, 4.6×150 mm I.D., 5 µm particle size column was used for the analysis. OphA samples (20 µl) were injected into a water-acetonitrile (Aldrich) gradient with a flow rate of 0.5 ml/min. The gradient started with water-acetonitrile (85:15) mix, changed to water-acetonitrile (10:90) mix over 10 min, held the water-acetonitrile mix constant for 7 min, returned to the start conditions over 3 min and then equilibrated for 5 min prior to the next sample. The UV detector voltage was set to 236 nm. Under these settings OphA had a retention time of 14.7 min. A calibration curve for OphA concentration against peak area was prepared for each solvent used (DCM, ethanol, toluene) and R^2 values of 0.99 were obtained. The change in concentration of OphA from before loading to after loading within the particles was used to infer the loading of OphA by the particles (Eqs. 2 and 3)

$$\%\ uptake = \frac{area\ of\ \ OphA\ peak\ after\ loading}{area\ of\ \ OphA\ peak\ initally, prior\ to\ loading} \quad (2)$$

$$moles\ of\ \ OphA\ uptaken = \%\text{uptake} * c * V \quad (3)$$

where c is the initial concentration of OphA prior to loading and V is the volume of loading solvent.

Release of OphA from HMSNP and PS-HMSNP

The release of OphA from the HMSNP@OphA and PS-HMSNP@OphA was monitored *in chemico* over 24 h. HMSNP@OphA loaded in DCM, ethanol or toluene (2.5 mg) or PS-HMSNP@OphA loaded in DCM (2.5 mg) were resuspended in 0.5 ml of PBS and placed on a rocking table at room temperature. HMSNP@OphA and PS-HMSNP@OphA samples were centrifuged at 12,000 rpm for 5 min to pellet the particles and then 20 µl of the supernatant was removed for further analysis. An equal volume of PBS was added to the HMSNP@OphA and PS-HMSNP@OphA samples to maintain a constant volume of PBS throughout the experiment. Sampling occurred after 1, 4, 8 and 24 h incubation times. The removed supernatant was diluted in 180 µl of PBS and then the concentration of OphA within the sample was determined by LC using the same setup as described in "Loading of OphA into the HMSNP and PS-HMSNP". Experiments were performed in triplicate on three separate occasions.

Degradation of OphA

The degradation of free OphA was monitored *in chemico* over 72 h. OphA was resuspended in 2 ml of PBS at a concentration of 0.1 mg/ml. Samples (250 µl) were taken after 0, 24, 48 and 72 h and analysed by LC (as described in Loading of OphA into the HMSNP and PS-HMSNP). OphA degradation peaks were observed at Rt=13.3, 14.5, 15.5 and 15.9 min.

Statistical Analysis

The data is presented as mean ± standard deviation (SD). Statistical analysis was performed by a one tailed students *t*-test in excel. $p<0.05$ was taken as the criteria for statistical significance.

RESULTS AND DISCUSSION

OphA Induces Apoptosis in RD Cells

Ophiobolin A was assessed in terms of its ability to effect cell death in Rhabdomyosarcoma (RD) cells. Morphologically RD cells in culture present as a spindle shape with large multinucleated cells (Fig. 2a). Incubation of the cells with 10 µM OphA for 24 h caused cells to round up and become more spherical. Cytoplasmic shrinkage could also be seen, along with membrane blebbing (Fig. 2b). To further interrogate the mechanism of action of OphA on RD cells, an inhibitor of actin polymerisation, Cytochalasin D (CytoD) was employed (20,21). Incubation of RD cells with CytoD alone was shown to induce microfilament formation (Fig. 2c). Combination of OphA and CytoD, however, resulted in RD cells which still exhibited the characteristic spherical shape, membrane blebbing and cytoplasm shrinkage seen in cells treated only with OphA (Fig. 2d).

To investigate the mechanism of cell death in RD cells exposed to OphA, cells were tagged with fluorescent markers

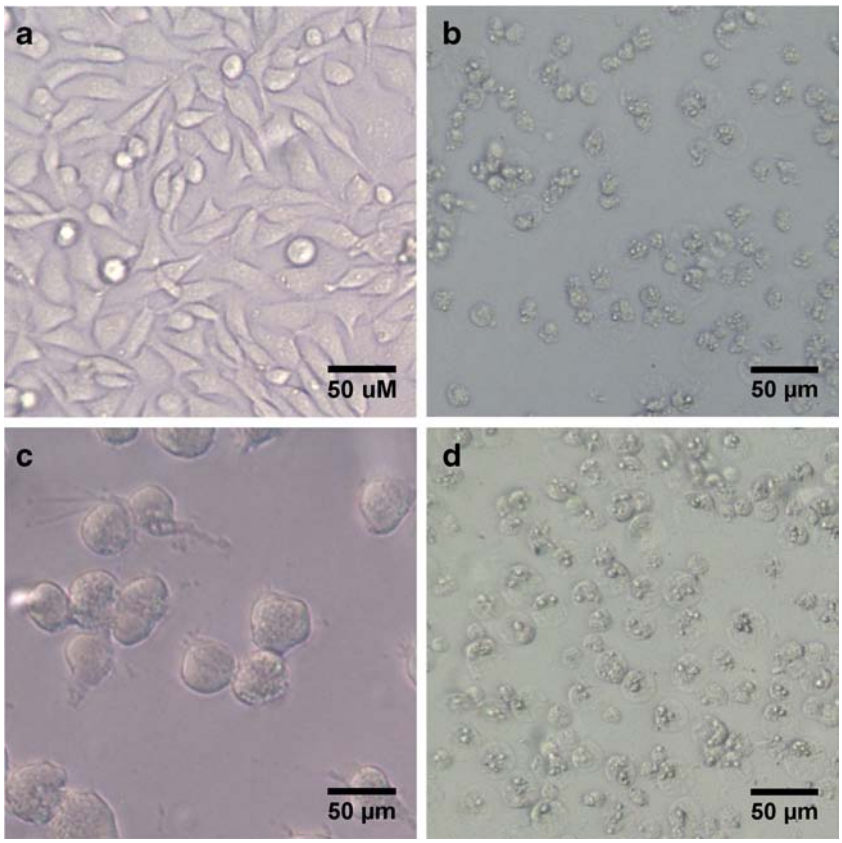

Fig. 2 Representive bright field images of RD cells with different treatments applied. (**a**) RD cells treated with PBS as a control, (**b**) RD cells treated with 10 μM OphA showing the cells rounding up and becoming more spherical. Blebbing at the membrance surface and cytoplasmic shrinkage can be seen due to the presence of OphA. (**c**) RD cells treated with 5 μM Cytochalasin D (CytoD) showing microtuble formation due to the inhibition of actin polymerisation caused by CytoD. (**d**) RD cells treated with 10 μM OphA plus 5 μM (CytoD) showing that the OphA still causes cells to round up and the membrane to bleb. Scale bars are all 50 μm.

and analysed by flow cytometry. The fluorophores used were propidium iodide (PI), a membrane impermeant dye that is generally excluded from viable cells, and APC-Annexin V. Annexin V binds to phosphatidylserine, a cell surface marker of apoptotic cells and therefore indicates cells undergoing early apoptosis. Cells stained with both fluorochromes are deemed to be late apoptotic, those stained with PI only to be necrotic, and cells stained with neither fluorophore to be viable. Representative scatter plots of PI and APC fluorescence for RD cells treated with 0, 1, 10 or 100 µM OphA for 24 h are shown in Fig. 3a. Cells can be seen to fall into distinct groups and these were used to gate for live, early apoptotic and dead cells. Low concentrations of OphA (1 µM) induced early apoptosis in RD cells (Fig. 3a (ii)) while 10 and 100 µM OphA showed late apoptotic or dead cells (Fig. 3a (iii) and (iv)). Quantification of the data showed that treatment with 10 µM OphA showed a peak in the percentage of apoptotic cells (Fig. 3b). Treatment with 100 µM caused all the cells to have died via apoptosis when the samples were analysed (Fig. 3b).

The IC_{50} of OphA on RD cells after 24 h treatment is between 1 and 2 µM (Fig. 3b). This is higher than previously reported IC_{50} values for OphA on a number of different cell lines, (8,9) however, these studies all applied the OphA treatment for 3 days rather than 24 h which could explain the higher level of IC_{50} found in this study.

Previously Bury *et al.* (13) found that GBM cells incubated with OphA did not show Annexin V binding and therefore cell death proceeded via paraptosis rather than apoptosis. This difference could be accounted for because GBM cells are known to have a defective apoptotic signalling pathway meaning they are resistant to apoptosis, (22) whereas there are many reports showing that apoptosis can be induced in RD cells (23,24). Another plant derived compound, honokiol, has been shown to induce paraptosis in NB4 and K562 leukaemia cell lines at low concentrations (25). In those cells where vacuoles were observed in the cytoplasm, a hallmark of paraptosis, no annexin V binding was observed. However at higher concentrations, honokiol induced apoptosis and necrosis. Therefore, apoptosis could have been observed in this study because higher concentrations of OphA were used than by Bury *et al.* (13) or because RD cells have a greater propensity to die via apoptosis.

OphA Increases Microvesicle Production and Size

Nanoparticle tracking analysis (NTA) was used to further investigate membrane blebbing effects in terms of microvesicle production. A representative NTA trace of microvesicle concentration *versus* microvesicle size shows the increase in microvesicle production after treatment with 1 µM OphA

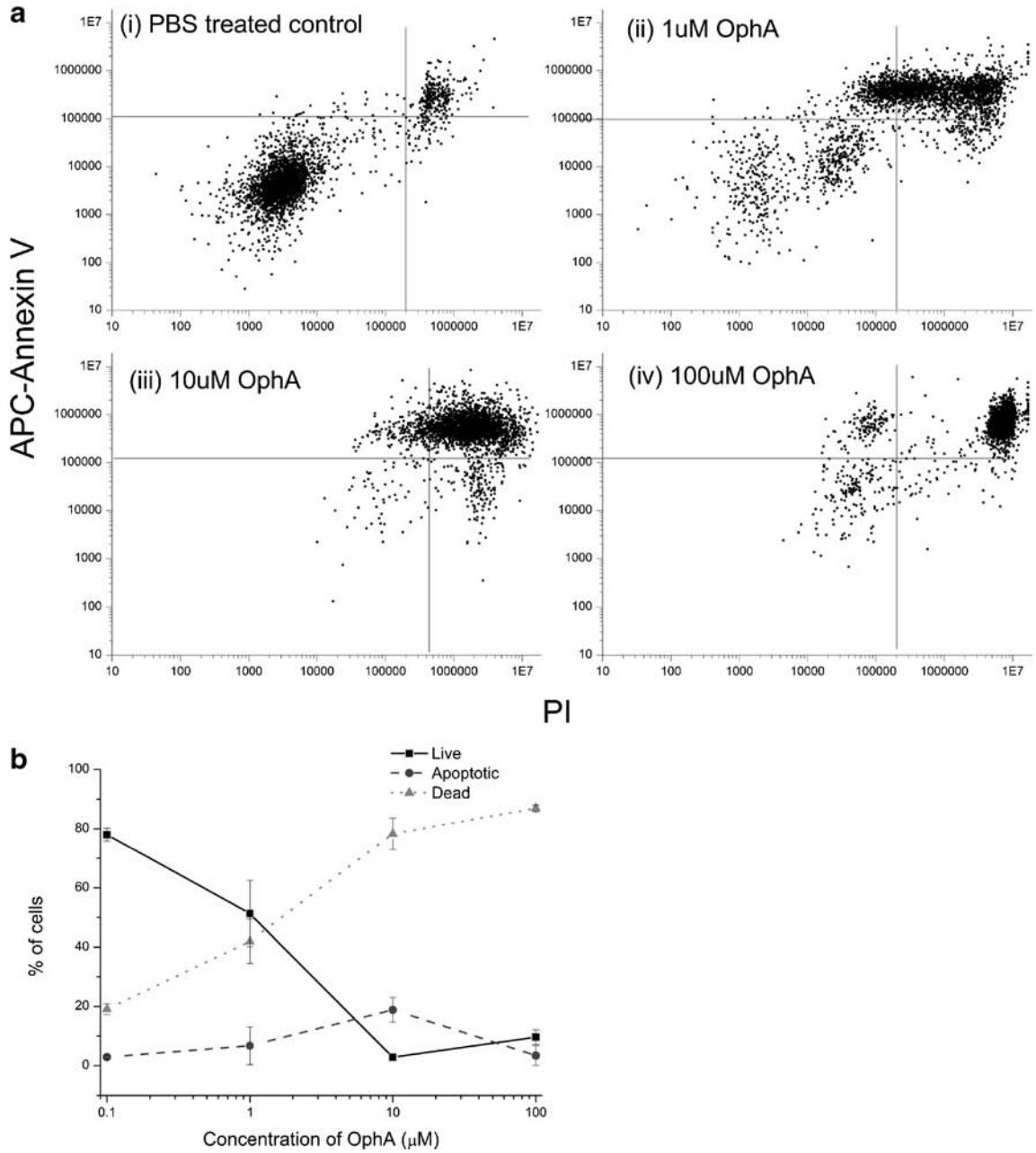

Fig. 3 Effect of OphA on cell viability measured by flow cytometry. (**a**) Representative flow cytometry results for RD cells treated with 0–100 μM OphA illustrating the cell staining with PI and APC-Annexin V. High PI fluorescence shows dead cells while high APC-Annexin 5 fluorescence show apoptotic cells, live cells show no fluorescence in these channels. (**b**) Representative results from $n = 3$ independent experiments showing the percentage of live, apoptotic and dead cells. Data is presented at mean ± SD.

for 24 h (Fig. 4a). There was a significant increase ($p < 0.05$) in the concentration of microvesicles produced from (72 ± 6) to $(180 \pm 31) \times 10^8$ microvesicles/ml after treatment with 1 μM OphA compared to the control (Fig. 4d). There was a very significant ($p < 0.005$) increase from (72 ± 6) to $(170 \pm 11) \times 10^8$ microvesicles/ml in the concentration of microvesicles produced after treatment with 10 μM OphA (Fig. 4d) compared to the PBS only treated control. Microvesicle release in response to drug has been observed previously, for example, Shedden *et al.* (26) observed that doxorubicin could be found in microvesicles after treatment and the rate of vesicle shedding was proportional to doxorubicin resistance across various cell lines.

There was a slight shift in the mode, mean and peak size of the microvesicles produced due to OphA treatment (Table I). The mode microvesicle size increases from 117 nm (control) to 126 nm (1 μM OphA) or 121 nm (10 μM OphA), mean microvesicle size increases from 158 nm (control) to 160 nm

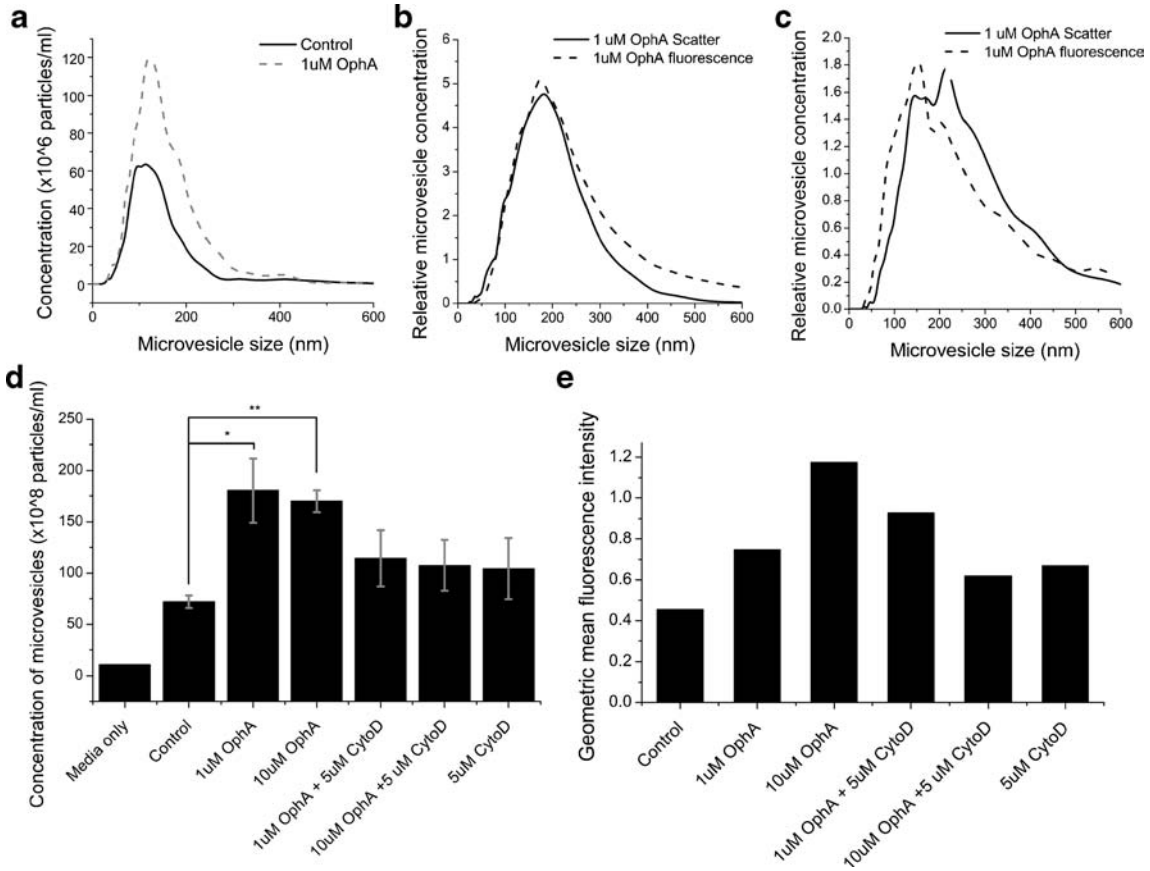

Fig. 4 Effect of OphA and CytoD on microvesicle production. (**a**) Representative nanoparticle tracking analysis trace showing the change in microvesicle concentration with microvesicle size for PBS control treated cells and cells treated with 1 μM OphA. (**b**) Representative fluorescence nanoparticle trace (cells treated with 1 μM OphA) showing that microvesicles produced can be stained with CellMaskTM orange showing that the shed microvesicles originate from the plasma membrane. (**c**) Representative fluorescence nanoparticle trace (cells treated with 1 μM OphA) showing that microvesicles produced can be stained with SYBR® green suggesting that they contain DNA. (**d**) Representative results from an independent experiment showing the change in microvesicle concentration after different treatments (PBS only, 1 and 10 μM OphA, 1 and 10 μM OphA plus 5 μM CytoD and 5 μM CytoD only) $n = 3$. Data is presented at mean ± SD of triplicate samples and significance was tested using a one tailed *t*-test (*$p < 0.05$, **$p < 0.005$). (**e**) Representative results from an independent experiment showing the fluorescence intensity of SYBR® green stained microvesicles indicating the presence of DNA in the microvesicles. Data is presented as the geometric mean fluorescence intensity.

(1 μM) or 189 nm (10 μM) and peak microvesicle size increases from 115 nm (control) to 122 nm (1 μM) or 121 nm (10 μM) (Table I). Since OphA induces apoptosis in RD cells this could be due to apoptotic bodies forming as a result of the OphA treatment, and hence the increase in microvesicle size.

Cytochalasin D Prevents the Release of Large Microvesicles

CytoD is often used in combination with a drug to further probe its mechanism of action (27,28). In this study CytoD was used to investigate whether changes in the cytoskeleton affect

Table I Effect of OphA and CytoD on Microvesicle Size. Representative Results from an Independent Experiment Showing the Mode, Mean and Peak Microvesicle Size

	Mode microvesicle size (nm)	Mean microvesicle size (nm)	Peak microvesicle size (nm)
PBS only treated RD cells	117	157.92	115
1 μM OphA treated RD cells	125.8	160.15	122
10 μM OphA treated RD cells	121.2	180.22	121
1 μM OphA +5 μM CytoD treated RD cells	127.2	170.06	115
10 μM OphA +5 μM CytoD treated RD cells	111.6	142.48	97
5 μM CytoD treated RD cells	116.2	171.56	115

microvesicle production. In the presence of CytoD only there is no significant increase in the number of microvesicles produced above the control, (72 ± 6) and $(104 \pm 30) \times 10^8$ microvesicles/ml (Fig. 4d). The mode and peak microvesicle size observed for CytoD treated cells are 116 nm and 115 nm, respectively (Table I). Thus there is no significant change from the mode (117 nm) and peak microvesicle size (115 nm) produced by the PBS control (Table I). This indicates that CytoD does not have any significant effect on the production of microvesicles under normal culture conditions. When cells are incubated in a combination of OphA and CytoD, both the number and size of the microvesicles produced is the same as that observed in the PBS only control (Fig. 4d, Table I). This indicates that the CytoD inhibits the formation of the larger apoptotic bodies but the smaller constitutively expressed exosomes, as seen in the control, are still produced. Thus our results are in line with the proposed mechanism whereby the actin-myosin system is the source of contractile force which drives both membrane blebbing and apoptotic body formation, (29) and this is prevented by the inhibition of actin polymerization with CytoD. Previous work has shown that CytoD (10 μM) inhibits microvesicle formation from activated platelets by 70% (30) and Cytochalasin B, which also inhibits actin polymerisation prevents the formation of 200–800 nm microvesicles from leukocytes (31).

Microvesicles Originate from the Plasma Membrane

To determine the origin of the microvesicles, samples were stained with CellMask^{TM} orange; a fluorescent dye which stains the plasma membrane. Signals from both light scatter (showing the total number of microvesicles) and fluorescence (showing the number of fluorescently labelled microvesicles) were recorded by NTA. A representative NTA trace, showing the scatter and fluorescence signal for cells treated with 1 μM OphA has been provided (Fig. 4b). This shows that there is a good agreement between the scatter and fluorescence signals indicating that the majority, >86%, of the microvesicles were stained with the CellMask^{TM} orange and hence they originated from the plasma membrane.

Microvesicles Contain DNA

Apoptotic bodies are known to contain DNA and therefore we used SYBR® green, a nucleic acid stain which preferentially stains double stranded DNA, to determine if the shed microvesicles contained DNA. This was done using fluorescence NTA using a similar method as for the CellMask^{TM} orange. There was good agreement between the scatter and fluorescence traces which suggests that the DNA is found within the shed microvesicles and not in larger cell debris (Fig. 4c). However, not all the microvesicles were stained with SYBR® green which indicated that not all the microvesicles contained DNA (Fig. 4e). There was an increase in the fluorescence intensity by 164% (1 μM OphA) and 258% (10 μM OphA) compared to the PBS only control treated cells (Fig. 4e). A smaller increase of 147% was observed in the cells treated with CytoD only. This suggests that the cells are releasing more DNA under stress conditions (32) or during apoptosis. Guescini *et al.* showed both glioblastoma cells and astrocytes constitutively release exosomes containing mitochondrial DNA (mtDNA) (33). Additionally, Bergsmedh *et al.* (34) and Waldenström *et al.* (35) have both shown that DNA contained within either tumour apoptotic bodies or shedding microvesicles can be taken up by fibroblast cells. This suggests that cells may be releasing DNA within microvesicles as a means of cell-to-cell signalling. Here, the highest DNA release was seen in the cells which were treated with the highest concentration of OphA and would likely be under the most stress.

Chemoembolic Particles for Targeted Drug Delivery

OphA has therefore been shown to be an effective chemotherapeutic both here and in previous studies; however, to avoid off-target effects it is optimal to deliver the therapeutic at the site of action. Novel composite embolic particles (PS-HMSNP) have been designed comprising a polystyrene microsphere (PS) at the core, covered with mesoporous silica nanoparticles (HMSNP) to create a shell layer (Fig. 5a). The PS core has been designed to effectively obstruct the tumour vasculature, while the HMSNP shell can be loaded with drug. The chemoembolization particles allow the drug to be delivered directly at the tumour location.

The mesoporous silica particles were examined by TEM (Fig. 5b) and SEM (Fig. 5c) and shown to have a hexagonal arrangement of the pores channels, and the overall shape to be roughly spherical with a slight elongation of the nanoparticles in the direction of the channels. The HMSNPs were determined to be approximately 120 nm in diameter, with a pore diameter of approximately 2 nm. Another study from our group measured a large sample of these HMSNPs and the nanoparticles were shown to be (105.66 ± 23.11) nm ($n=431$) and to have a pore size of (2.13 ± 0.21) nm ($n=544$) (36). The mean hydrodynamic diameter of the HMSNP was determined to be 120 nm by disc centrifugation; which is similar to the diameter measured by TEM. The zeta potential of the HMSNP was (-39 ± 1) mV at pH7, and therefore at physiologically relevant pH values the nanoparticles are stable (electrokinetic (ζ) potential <-30 mV), and will form a stable suspension without aggregation.

As a basis for the embolic particles, polystyrene spheres were synthesized and used as a carrier for the HMSNP. The polystyrene spheres were synthesised by the copolymerization

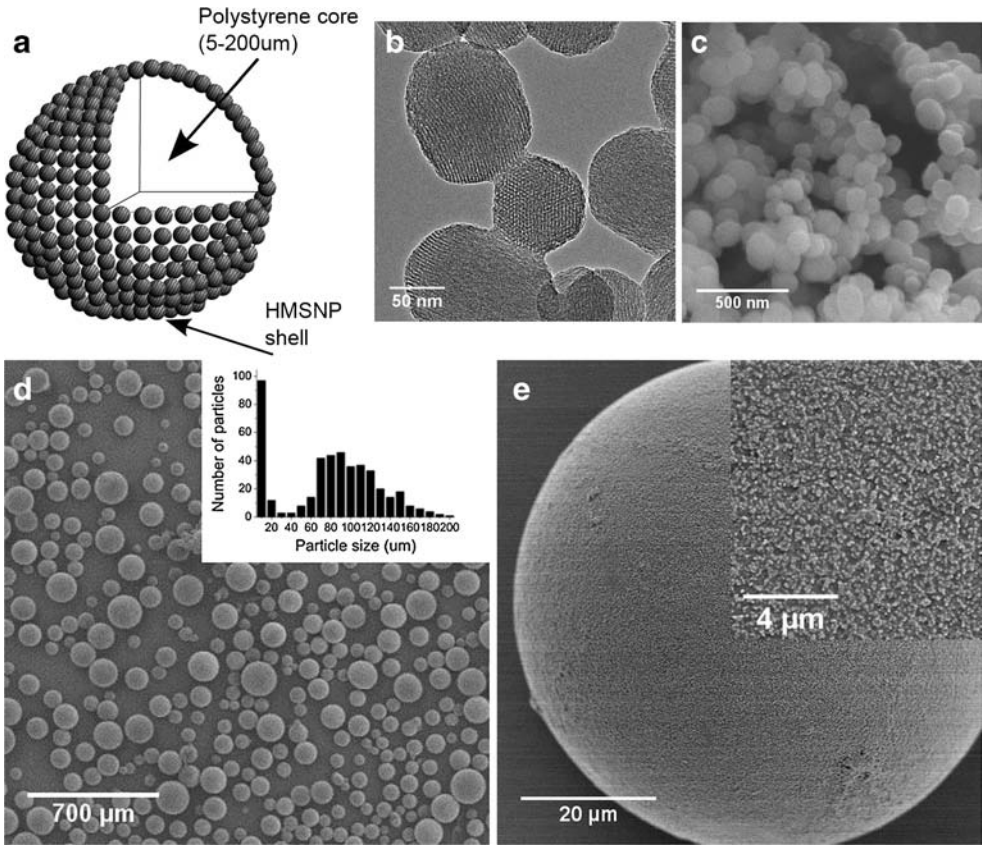

Fig. 5 Electron microscopy images of the as synthesized HMSNP and PS-HMSNP. (**a**) Schematic of the prepared PS-HMSNP chemoembolization particles. The polystyrene core acts an embolic agent obstructing the tumour vasculature and the HMSNP shell can be loaded with a chemotherapy drug (Image not to scale) (**b**) TEM image of the HMSNP showing the size and hexagonal orientation of the pores (scale bar: 50 nm). (**c**) SEM image of the HMSNP (3 kV, scale bar: 500 nm). (**d**) SEM image of the PS-HMSNP and insert showing the size dispersion of the PS particles (3 kV, scale bar: 700 μm). (**e**) SEM image of the PS-HMSNP microparticle (3 kV, scale bar: 20 μm) and insert showing the HMSNP on the surface of the polystyrene microparticle (3 kV, scale bar: 4 μm).

of styrene with ethylene glycol dimethacrylate, and the reaction was initiated by AIBN as described by Ihara *et al.* (16,17). Based on the reactivity ratios for styrene and ethylene glycol dimethacrylate (37), the copolymer is calculated to contain 55% styrene monomers and 45% ethylene glycol dimethacrylate monomers. The synthesised PS-HMSNP are very polydisperse with particles ranging from 5 µm to 200 µm with a large number of small, <10 µm, particles and a second peak at 90 µm (Fig. 5d; insert). This range of sizes will allow good blockage along the vasculature tree as the blood vessels narrow as they get closer to the tumour (Morrison *et al.*, in preparation). The coverage of the PS with HMSNP was optimised by changes in both the duration and temperature of sintering. Samples were assessed using SEM and good coverage of the PS-HMSNP was observed in samples sintered at 230°C for 2 h (Fig. 5e).

High Loading of OphA into the Pores of HMSNP and PS-HMSNP

Successful loading of OphA into the pores of the mesoporous silica is required for the drug to be carried by the embolic

Table II Loading and Release of OphA into PBS from HMSNP and PS-HMSNP. The Table Details the Percentage Loading OphA into the Particles Depending on the Solvent it was Loaded in, the Absolute Number of Moles of OphA per mg of HMSNP and the Maximum Moles of OphA Released from the Particles After 24 h in PBS

	HMSNP in DCM	HMSNP in Ethanol	HMSNP in toluene	PS-HMSNP in DCM
Proton acceptor solubility parameter of the solvent	0.5	5	0.5	0.5
% loaded based change in area of the OphA peak measured using liquid chromatography	94.6 ± 5.1	38.1 ± 4.2	95 ± 1.4	95.4 ± 6.2
Moles of OphA loaded per mg of HMSNP (μmoles)	23.7 ± 1.3	9.5 ± 1.1	23.8 ± 0.4	23.8 ± 1.6
Moles of OphA released after 24 h per mg of HMSNP (μmoles)	9.2 ± 2.3	0.6 ± 0.3	11.6 ± 0.2	3.9 ± 0.9
% moles released after 24 h	38.8	6.3	48.7	16.4

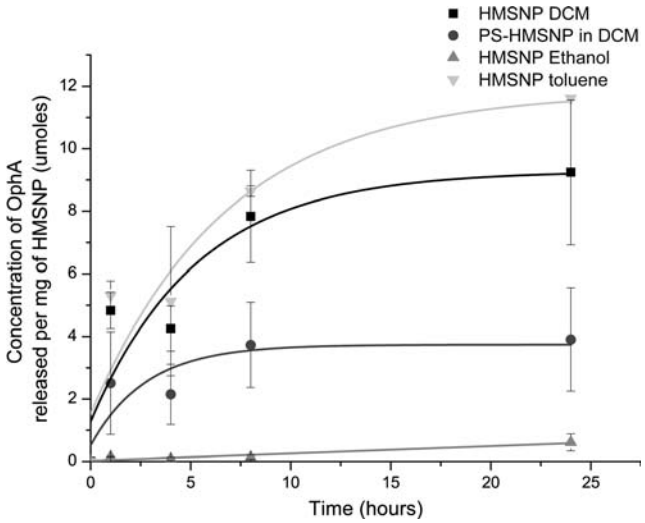

Fig. 6 Representative release profiles of OphA into PBS from the HMSNP and PS-HMSNP from an independent experiment. Data is presented as mean ± SD of triplicate samples.

particles. Liquid chromatography was used to monitor the loading of OphA into the pores of both HMSNP and PS-HMSNP. A number of solvents were trialled for drug loading; the highest loading of OphA was found in dichloromethane (DCM) (95%) and toluene (95%) whereas ethanol (38%) showed poor loading (Table II). This is due to the solubility of OphA in each solvent and their respective solubility parameters (Table II). The proton acceptor solubility parameter indicates the degree of dissolving of alcohol, phenol and carboxylic acid functional groups. OphA has both hydroxyl groups and carbonyl groups which allow for hydrogen bonding, hence it has a good affinity for solvents with high solubility parameters of proton acceptors like ethanol (5). DCM and toluene have low solubility parameters of proton acceptors (0.5), therefore the OphA had a greater interaction with the silanol groups in the mesoporous silica than the solvent and hence the OphA was adsorbed into the pores of the silica (38). Although loading HMSNP with OphA in toluene was successful, this could not be used for loading of OphA into

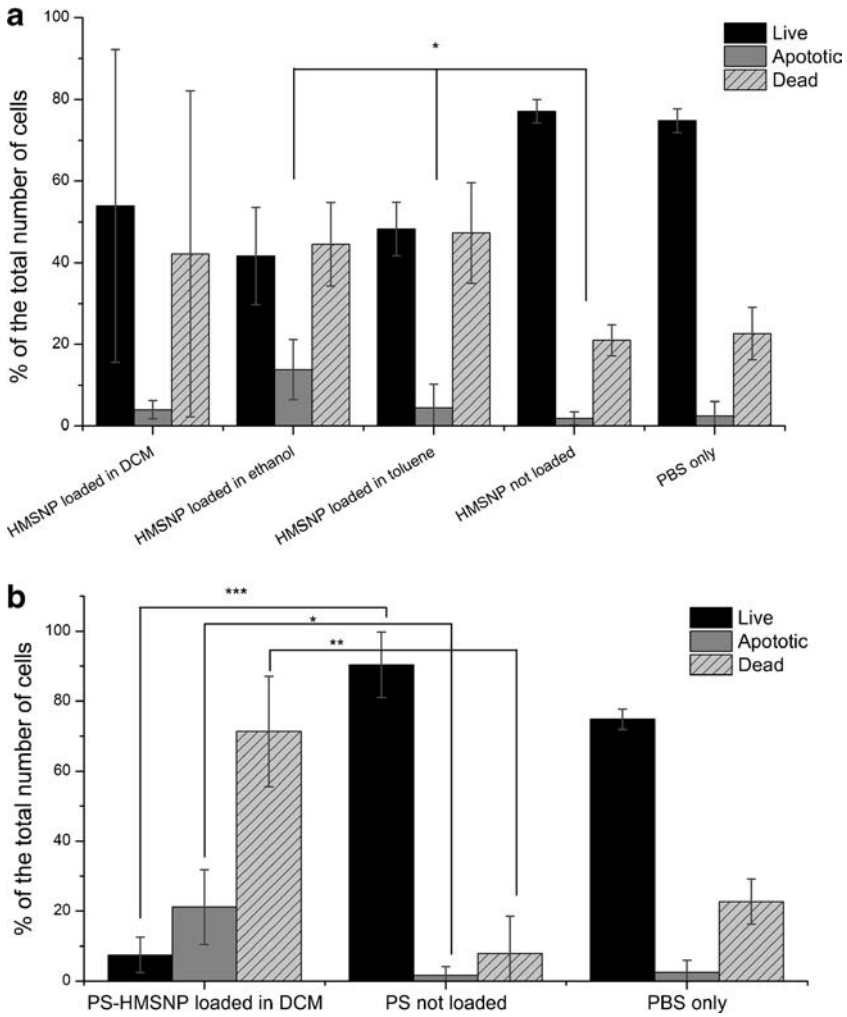

Fig. 7 Showing the ratio of live, apoptotic and dead cells after the release of OphA from loaded HMSNP and PS-HMSNP into RD cells. (**a**) Results from the mean of three experiments showing the ratio of live, apoptotic and dead cells after treatment with HMSNP loaded in DCM, ethanol and toluene. (**b**) Representative results from an independent experiment showing the ratio of live, apoptotic and dead cells after treatment with PS-HMSNP loaded with OphA. Data is presented as mean ± SD and significance was tested using a one tailed *t*-test (*$p < 0.05$, **$p < 0.005$, ***$p < 0.0005$).

PS-HMSNP since it causes the polystyrene to swell and degrade (39) and therefore the integrity of the PS-HMSNP would not be maintained.

Successful Release of OphA from HMSNP and PS-HMSNP

Good temporal release of OphA from the pores of the mesoporous silica is required to ensure that sustained drug delivery will be achieved. OphA has been successfully released from the pores of HMSNP both *in chemico* into PBS and *in vitro* onto RD cells grown in complete growth media. Release was shown in all the samples with the full cargo being released after approximately 24 h (Fig. 6). The highest release was observed for the samples loaded in toluene and DCM both in terms of absolute moles released and as a percentage of the total number of moles adsorbed into the silica pores (Table II). Samples loaded in toluene released 11.6±0.2 μmoles of OphA per mg of HMSNP over 24 h, while samples loaded in DCM released 9.2±2.3 μmoles of OphA per mg of HMSNP (Fig. 6). This equates to 49% and 39% release of the total encapsulated OphA for samples loaded in toluene and DCM respectively over the duration of the experiment. Poor release was observed in the HMSNP loaded in ethanol, with only 0.6±0.3 μmoles OphA per mg of HMSNP, which is only 6.3% of the total encapsulated cargo. The relative size of the drug compared to the pore size of the silica will also affect its loading and unloading profile. A large ratio of pore size to drug molecule size results in a high release rate whereas a small ratio will result in a sustained release due to the confinement effect of the pore (40).

Flow cytometry was used to determine the *in vitro* effect of cell death due to the release of OphA from the HMSNP and the PS-HMSNP on RD cells in growth media. There was a significant ($p<0.05$) decrease in cell viability after treatment with HMSNP@OphA loaded in either ethanol or toluene compared with unloaded control HMSNP (Fig. 7a). The number of live cells was reduced by 46% and 37% for cells treated with HMSNP@OphA loaded in either ethanol or toluene respectively. The *in vitro* results from the release of OphA from PS-HMSNP showed a very significant ($p<0.0005$) reduction in cell viability, approximately 70%, compared to the blank PS.

There was no significant difference between the unloaded control HMSNP or the PS particles and the PBS control which suggests that both the HMSNP and the PS are not toxic to the cells without the presence of the drug (Fig. 7b). This shows good biocompatibility of the developed drug delivery system which only causes cell death when OphA is present.

HMSNP Protects OphA from Degradation

One of the limiting factors in the clinical development of OphA is its poor chemical stability. The stability of the free drug in PBS was monitored by liquid chromatography over a period of 72 h (Figure S1). During this time the OphA peak area reduced by 75% and the main degradation products were observed at retention times of 13.3, 14.5, 15.5 and 15.9 min (Fig. 8a). These products have been previously identified by Bury *et al.* (8), and the main OphA degradation product was shown to be 3-anhydro-6-epi-ophiobolin A, which was significantly less potent than OphA itself.

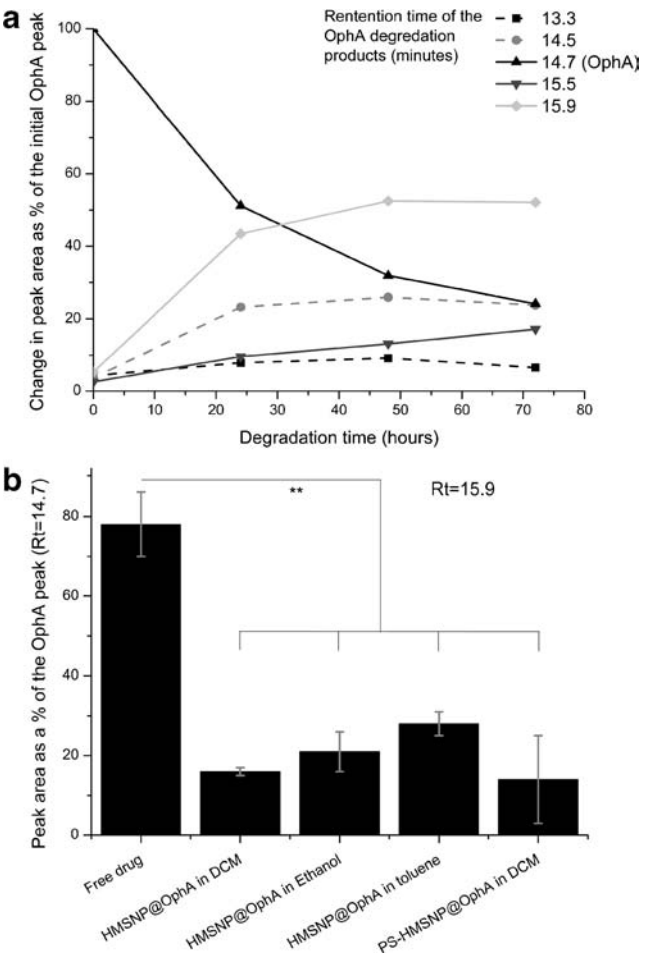

Fig. 8 Degradation of OphA. (**a**) Representative results from an independent experiment showing the degradation of 0.1 mg/ml free OphA (Rt = 14.7 min) to 4 main degradation products at Rt = 13.3, 14.5, 15.5 and 15.9 min. Data is presented as the change in peak area as a percentage of the OphA peak at the start of the experiment. (**b**) Representative results from an independent experiment showing the degradation of OphA after 24 h release from the HMSNP@OphA and PS-HMSNP@OphA. The largest degradation peak was observed at Rt = 15.9 min. Data is presented as the mean ± SD of the ratio of the peak area for OphA to the peak area for Rt = 15.9 min and significance was tested using a one tailed *t*-test (**$p < 0.005$).

Interestingly, the OphA released from the HMSNPs has undergone significantly less degradation compared to free OphA. After 24 h release from the HMSNP@OphA and PS-HMSNP@OphA the largest degradation product for all samples occurred at Rt=15.9 min (Fig. 8b). Quantifying the ratio of this peak area to that of the OphA peak area (Rt-14.7 min) showed a very significant ($p>0.005$) reduction in degradation of OphA for the HMSNP@OphA (16%±1, 21%±5 and 28%±3 for samples loaded in DCM, ethanol or toluene respectively) and PS-HMSNP (14%±11 for sample loaded in DCM) compared to the free drug (78%±8). Therefore we have shown that nanoparticles can be used to successfully protect a fragile chemical molecule and therefore increase its half-life within the body. Other studies, such as those of Karve *et al.* (41), where wortmannin was loaded into lipid polymer nanoparticles, show an increase in the stability of the molecules upon encapsulation.

CONCLUSIONS

In conclusion, we have designed and synthesised a chemoembolic particle which has a high surface area for loading with a novel chemotherapeutic drug OphA. OphA has been shown to be effective at inducing apoptosis in an RMS cancer cell line causing the cells to round up, their membrane to bleb and the cytoplasm to shrink. Membrane blebbing caused an increase in the number microvesicles shed due to OphA treatment. The microvesicles were shown to originate from the plasma membrane and they contained DNA which may have implications in cell-to-cell signalling. Successful encapsulation of OphA into the designed drug delivery system was observed and good release *in chemico* was achieved. Furthermore, significant cell death was shown in RD cells exposed to the OphA loaded chemoembolic particles. Subsequent experiments will be performed to assess the efficacy of the particles in animal models.

ACKNOWLEDGMENTS AND DISCLOSURES

Xinyue Huang is thanked for the RD cells expressing GFP and Begbroke Nano is thanked for access to materials characterisation equipment. Neil Young is thanked for training and advice with regards to TEM. Dr. Maurizio Vurro and Maria Chira Zonno (Istituto di Scienze delle Produzioni Alimentari, CNR, Italy) are thanked for supplying culture filtrates of *Drechslera gigantea* as well as Dr. Fabiana Avolio (Dipartimento di Scienze Chimiche, Università di Napoli Federico II, Napoli, Italy) for her collaboration in Ophiobolin A purification. R. Morrison is funded by RCUK Digital Economy Programme grant number EP/G036861/1 (Oxford Centre for Doctoral Training in Healthcare Innovation). R. Kiss is a director of research with the Fonds National de la Recherche Scientifique (FNRS-FRS; Belgium). H. Townley would like to thank the Williams Fund for continuing support.

REFERENCES

1. Shin SW. The current practice of transarterial chemoembolization for the treatment of hepatocellular carcinoma. Korean J Radiol. 2009;10(5):425–34.
2. Liu X, Wan Sia Heng P, Li Q, Chan LW. Novel polymeric microspheres containing norcantharidin for chemoembolization. J Control Release. 2006;116(1):35–41.
3. Argyo C, Weiss V, Bräuchle C, Bein T. Multifunctional mesoporous silica nanoparticles as a universal platform for drug delivery. Chem Mater. 2014;26:435–51.
4. Slowing II, Vivero-Escoto JL, Wu C-W, Lin VSY. Mesoporous silica nanoparticles as controlled release drug delivery and gene transfection carriers. Adv Drug Deliv Rev. 2008;60(11):1278–88.
5. Au TK, Chick WSH, Leung PC. The biology of ophiobolins. Life Sci. 2000;67(7):733–42.
6. Chattopadhyay AK, Samaddar KR. Effects of Helminthosporium oryzae infection and ophiobolin on the cell membranes of host tissues. Physiol Plant Pathol. 1976;8(2):131–9.
7. Leung PC, Taylor WA, Wang JH, Tipton CL. Ophiobolin-A—a natural product inhibitor of calmodulin. J Biol Chem. 1984;259(5):2742–7.
8. Bury M, Novo-Uzal E, Andolfi A, Cimini S, Wauthoz N, Heffeter P, *et al.* Ophiobolin A, a sesterterpenoid fungal phytotoxin, displays higher in vitro growth-inhibitory effects in mammalian than in plant cells and displays in vivo antitumor activity. Int J Oncol. 2013;43(2):575–85.
9. de Vries-van Leeuwen IJ, Kortekaas-Thijssen C, Nzigou Mandouckou JA, Kas S, Evidente A, de Boer AH. Fusicoccin-A selectively induces apoptosis in tumor cells after interferon-α priming. Cancer Lett. 2010;293(2):198–206.
10. Giacalone PL, Deisseignet PH, Roger P, Taourel P, Vernet H, Laffargue F. Pre-operative arterial embolisation of a uterine rhabdomyosarcoma in a 14-year-old girl. Br J Radiol. 2004;77(920):701–3.
11. Sam J, Price S. Embolization of a perineal rhabdomyosarcoma in a patient with priapism and disseminated intravascular coagulation. Hospital of the University of Pennsylvania. 2014 January 11; Available from: http://members.sirweb.org/members/caseclub/0798/0798_10/0798_10.htm.
12. Nagulic M, Prstojevic B, Simic R, Majstorovic B, Nikolic I. Resection of orbital rhabdomyosarcoma in an infant with the aid of preoperative partial arterial embolization. A case report. Neuroradiol J. 2007;20(6):699–703.
13. Bury M, Girault A, Megalizzi V, Spiegl-Kreinecker S, Mathieu V, Berger W, et al. Ophiobolin A induces paraptosis-like cell death in human glioblastoma cells by decreasing BKCa channel activity. Cell Death Dis. 2013;4:1–11.
14. Simpson R, Mathivanan S. Extracellular microvesicles: the need for internationally recognised nomenclature and stringent purification criteria. J Proteome Bioinforma. 2012;5:ii.
15. Hom C, Lu J, Liong M, Luo H, Li Z, Zink JI, *et al.* Mesoporous silica nanoparticles facilitate delivery of siRNA to shutdown signaling pathways in mammalian cells. Small. 2010;6(11):1185–90.
16. Ihara H, Kubota S, Uchimura A, Sakai Y, Wakiya T, Rahman MM, *et al.* A facile preparation method for self-assembled monolayers with silica particles on polystyrene-based microspheres. Mater Chem Phys. 2009;114(1):1–5.

17. Uchimura A, Kubota S, Yamada S, Wakiya T, Takafuji M, Shirosaki T, *et al.* Facile and versatile method for preparing core—shell microspheres with controlled surface structures based on silica particles-monolayer. Mater Chem Phys. 2011;129(3):871–80.
18. Evidente A, Andolfi A, Cimmino A, Vurro M, Fracchiolla M, Charudattan R. Herbicidal potential of ophiobolins produced by drechslera gigantea. J Agric Food Chem. 2006;54(5):1779–83.
19. Kafri T, van Praag H, Gage FH, Verma IM. Lentiviral vectors: regulated gene expression. Mol Ther. 2000;1(6):516–21.
20. Fox JEB, Phillips DR. Inhibition of actin polymerization in blood platelets by cytochalasins. Nature. 1981;292(5824):650–2.
21. Casella JF, Flanagan MD, Lin S. Cytochalasin D inhibits actin polymerization and induces depolymerization of actin filaments formed during platelet shape change. Nature. 1981;293(5830):302–5.
22. Krakstad C, Chekenya M. Survival signalling and apoptosis resistance in glioblastomas: opportunities for targeted therapeutics. Mol Cancer. 2010;9(1):135.
23. Zhu G, Zheng Y, Zhang L, Shi Y, Li W, Liu Z, *et al.* Coxsackievirus A16 infection triggers apoptosis in RD cells by inducing ER stress. Biochem Biophys Res Commun. 2013;441(4):856–61.
24. Shi W, Li X, Hou X, Peng H, Jiang Q, Shi M, *et al.* Differential apoptosis gene expressions of rhabdomyosarcoma cells in response to enterovirus 71 infection. BMC Infect Dis. 2012;12(1):327.
25. Wang Y, Zhu X, Yang Z, Zhao X. Honokiol induces caspase-independent paraptosis via reactive oxygen species production that is accompanied by apoptosis in leukemia cells. Biochem Biophys Res Commun. 2013;430(3):876–82.
26. Shedden K, Xie XT, Chandaroy P, Chang YT, Rosania GR. Expulsion of small molecules in vesicles shed by cancer cells: association with gene expression and chemosensitivity profiles. Cancer Res. 2003;63(15):4331–7.
27. Gregoraszczuk EL, Stoklosowa S. The effect of microtubule and microfilament-disrupting drugs on prolactin-stimulated progesterone synthesis and secretion by cultured porcine theca cells. Acta Histochem. 1997;99(2):207–15.
28. Schliwa M. Action of cytochalasin D on cytoskeletal networks. J Cell Biol. 1982;92(1):79–91.
29. Coleman ML, Sahai EA, Yeo M, Bosch M, Dewar A, Olson MF. Membrane blebbing during apoptosis results from caspase-mediated activation of ROCK I. Nat Cell Biol. 2001;3(4):339–45.
30. Yano Y, Kambayashi JI, Shiba E, Sakon M, Oiki E, Fukuda K, *et al.* The role of protein phosphorylation and cytoskeletal reorganization in microparticle formation from the platelet plasma membrane. Biochem J. 1994;299:303–8.
31. Timár CI, Lőrincz ÁM, Csépányi-Kömi R, Vályi-Nagy A, Nagy G, Buzás EI, *et al.* Antibacterial effect of microvesicles released from human neutrophilic granulocytes. Blood. 2013;121(3):510–8.
32. Balaj L, Lessard R, Dai L, Cho Y-J, Pomeroy SL, Breakefield XO, *et al.* Tumour microvesicles contain retrotransposon elements and amplified oncogene sequences. Nat Commun. 2011;2:180.
33. Guescini M, Genedani S, Stocchi V, Agnati L. Astrocytes and Glioblastoma cells release exosomes carrying mtDNA. J Neural Transm. 2010;117(1):1–4.
34. Bergsmedh A, Szeles A, Henriksson M, Bratt A, Folkman MJ, Spetz A-L, *et al.* Horizontal transfer of oncogenes by uptake of apoptotic bodies. Proc Natl Acad Sci. 2001;98(11):6407–11.
35. Waldenström A, Gennebäck N, Hellman U, Ronquist G. Cardiomyocyte microvesicles contain DNA/RNA and convey biological messages to target cells. PLoS ONE. 2012;7(4):e34653.
36. Huang X, Young NP, Townley HE. Characterisation and comparison of mesoporous silica particles for optimised drug delivery. Nanomater Nanotechnol. 2014;4:2.
37. Frickm CD, Rudin A, Wiley RH. Reactivity ratios for divinylbenzene and ethylene glycol dimethacrylate copolymerizations with styrene and methyl methacrylate. J Macromol Sci A Chem. 1981;16(7):1275–82.
38. Hata H, Saeki S, Kimura T, Sugahara Y, Kuroda K. Adsorption of taxol into ordered mesoporous silicas with various pore diameters. Chem Mater. 1999;11(4):1110–9.
39. Zhang R, Cherdhirankorn T, Graf K, Koynov K, Berger R. Swelling of cross-linked polystyrene beads in toluene. Microelectron Eng. 2008;85(5–6):1261–4.
40. He Q, Shi J. Mesoporous silica nanoparticle based nano drug delivery systems: synthesis, controlled drug release and delivery, pharmacokinetics and biocompatibility. J Mater Chem. 2011;21(16):5845–55.
41. Karve S, Werner ME, Sukumar R, Cummings ND, Copp JA, Wang EC, *et al.* Revival of the abandoned therapeutic wortmannin by nanoparticle drug delivery. Proc Natl Acad Sci. 2012;109(21):8230–5.